ISA Transactions 57 (2015) 329–339

Contents lists available at ScienceDirect

ISA Transactions

journal homepage: www.elsevier.com/locate/isatrans

Modeling and simulation of soft sensor design for real-time speed and position estimation of PMSM

Ines Omrane [a,*], Erik Etien [a], Wissam Dib [b,1], Olivier Bachelier [a]

[a] Laboratoire d'Informatique et d'Automatique pour les Systémes (LIAS), Bâtiment B25, 2, rue Pierre Brousse, 86022 Poitiers, France
[b] IFP Energies Nouvelles, 1 & 4, avenue de Bois-Préau 92852 Rueil-Malmaison Cedex - Paris, France

ARTICLE INFO

Article history:
Received 1 October 2013
Received in revised form
3 June 2014
Accepted 11 June 2014
Available online 25 February 2015
This paper was recommended for publication by Dr. A.B. Rad

Keywords:
Design
Modeling
Simulation
Motor speed control
Soft sensor
Permanent magnet synchronous motor

ABSTRACT

This paper deals with the design of a speed soft sensor for permanent magnet synchronous motor. At high speed, model-based soft sensor is used and it gives excellent results. However, it fails to deliver satisfactory performance at zero or very low speed. High-frequency soft sensor is used at low speed. We suggest to use a model-based soft sensor together with the high-frequency soft sensor to overcome the limitations of the first one at low speed range.

1. Introduction

PMSM are receiving a very important attention in several industrial sectors because of its simplicity of design, ability of operation at high speeds, high efficiency and high power/torque density. For this reason, the sensorless control of a synchronous machine has been an interesting topic. The main idea of this approach is to replace the mechanical sensor by a soft sensor which offers a number of attractive properties one of them being a low cost alternative to hardware speed measurement used in classical motor drives [1–3]. For example, the cost of a sensor may exceed the cost of a small motor in some applications. Also, the presence of the mechanical sensors not only increases the cost and complexity of the total material with additional wiring but also reduces its reliability with additional sensitivity to external disturbances. In addition, it may be difficult to install and maintain a position sensor due to the limited space and rigid work environment with high vibration or high temperature.

At high speed, model-based soft sensors give excellent results. Several techniques inspired from control theory [4–6], such as adaptive observers [7–10], reference models [11–13], and extended Kalman filter [14]. Whatever the chosen method is, the sensor design procedure can be summarized by Fig. 1 [15]. However, these methods fail to deliver satisfactory performance at zero or very low speed. From a practical standpoint, the operational limit of these methods is typically $\omega_N/20$, with ω_N being the rated motor speed. So, high-frequency soft sensors are used in this velocity region. The estimated parameters are obtained from the carrier high frequency signal injection [16]. In most of these methods, a signal, which can be either a current or a voltage, is injected in the $(\alpha–\beta)$ or $(d–q)$ components. These techniques are usually applied to the interior permanent magnet synchronous motor (I-PMSM) as it involves the effect of salience [17]. In [18,19], signal injection method was extended to the surface permanent magnet synchronous motor (S-PMSM) by exploiting the saliency resulting from magnetic saturation.

An attractive solution is to combine the two sensors to obtain a full-speed range operation. Several hybrid method have been presented in the literature [20–25]. In [21,22], the changeover algorithm was performed using weighting coefficients. A linear combination between the position estimates at high and low speeds was used in [23] to get a smooth transition. In [24], the method of transition consists in using a weighted average of the

* Corresponding author. Tel.:+33 5 49 45 35 08; fax: +33 5 49 45 40 34.
E-mail addresses: ines.omrane@univ-poitiers.fr (I. Omrane), erik.etien@univ-poitiers.fr (E. Etien), wissam.dib@ifpen.fr (W. Dib), olivier.bachelier@univ-poitiers.fr (O. Bachelier).
[1] Tel.: +33 1 47 52 60 00; fax: +33 1 47 52 70 00.

http://dx.doi.org/10.1016/j.isatra.2014.06.004

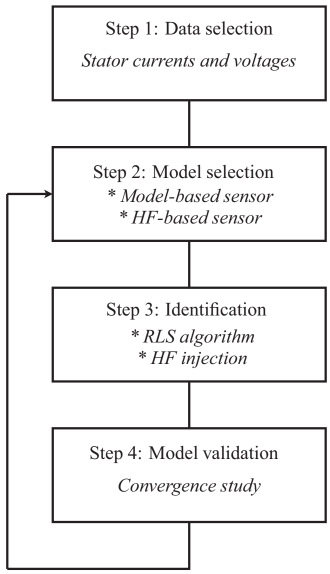

Fig. 1. Soft sensor development.

estimated speed and position in a given speed gap. In [25], the incorporation of the HF quantities estimates in the flux observer allowed a smooth transition and an improvement of the feedback signal quality.

To ensure that model-based soft sensor works properly, the PMSM model and its parameters must be known. For this, a sensorless parameter identification is required. In this paper, a simple identification procedure, based on HF signal injection and exploiting the implementation of state variable filters which replace the band-pass filters, used in the HF signal injection technique, to obtain a linear model with respect to the parameters is used. Thus, a least squares algorithm is applied to identify the model parameters.

In this paper, we suggest to use a model-based soft sensor together with the high-frequency soft sensor to overcome the limitations of the first one at low speed range. A simple identification procedure based on HF signal injection and exploiting the implementation of state variable filters is developed. In order to validate the proposed soft sensor, we provide several simulation results to assess the relevancy of the proposed solution. The main interest of this soft sensor is its simplicity, which makes it a suitable candidate for practical implementation.

Appropriate assumptions allow us to neglect nonlinear effects as saturations, iron losses or magnetic hysteresis in order to derive a simplified physical model. It yields a good approximation of the motor behavior which is sufficient for control objectives. The identification step concerns the determination of model parameters. In Section 3, the general formulation of the recursive least squares algorithm is shown. The final step towards the identification is the validation (Section 4). This phase requires us to verify whether the model is able to adequately represent the system. If the validation test fails, the soft sensor design should be reconsidered.

2. Model selection

2.1. Motor model

In this section, the model of PMSM is presented in two different frames: in the stationary reference frame (α–β) and in the rotating frame (d–q).

2.1.1. Model in the stationary reference frame (α–β)

The unsaturated PMSM can be modeled in the stationary reference frame (α–β) by the following set of equations [26]:

$$L\frac{di_{\alpha\beta}}{dt} = -R_s i_{\alpha\beta} + \omega_e \psi_{pm}\begin{bmatrix} \sin(\theta_e) \\ -\cos(\theta_e)\end{bmatrix} + u_{\alpha\beta} \tag{1}$$

$$T_e = \frac{3p}{4}\psi_{pm}(i_\alpha \cos(\theta_e) - i_\beta \sin(\theta_e)) \tag{2}$$

where $i_{\alpha\beta} = \left[i_\alpha \ i_\beta\right]^T$ is the stator current vector, $u_{\alpha\beta} = \left[u_\alpha \ u_\beta\right]^T$ is the motor terminal voltage vector, R_s is the stator windings resistance, L is the cyclic inductance, ψ_{pm} is the magnetic flux, p is the number of pole pairs, θ_e is the electrical rotor position and ω_e is the electrical rotor speed. Throughout this paper, we shall assume that the mechanical parameters, position and speed, are unknown.

2.1.2. Model in the rotating frame (d–q)

This model is obtained by implementing Park's transform to Eqs. (1) and (2). Then, PMSM can be given by

$$\begin{aligned} L\frac{di_d}{dt} &= -R_s i_d + u_d + \omega_e L i_q \\ L\frac{di_q}{dt} &= -R_s i_q + u_q - \omega_e\left(L i_d + \psi_{pm}\right) \\ T_e &= p\psi_{pm} i_q \end{aligned} \tag{3}$$

In this type of model, the delivered torque T_e is proportional to the quadrature current i_q. Thereby, this representation is the most frequently used in the field-oriented control of PMSM. However, Park's transform requires the use of the electrical position which is not available in sensorless applications. Several techniques have been developed to estimate, in a first step, the velocity from which we can deduce the position by integration.

2.2. Sensor model

This section deals with the estimation of the rotor position at high speeds. The presented technique is based on the model of the PMSM given by (1) and (2) and on an online reconstruction of the back-electromotive force [27].

Let us define $\Psi_{\alpha\beta} = \left[\Psi_\alpha \ \Psi_\beta\right]^T$ by

$$\Psi_{\alpha\beta} = L i_{\alpha\beta} + \psi_{pm}\begin{bmatrix}\cos(\theta_e) \\ \sin(\theta_e)\end{bmatrix} \tag{4}$$

Based on the previous equation, we can obtain the rotor position

$$\theta_e = a\tan 2(\Psi_\beta - L i_\beta, \Psi_\alpha - L i_\alpha) \tag{5}$$

But in the sensorless control, the position is unknown so we cannot compute the actual value of the total flux. As a solution, we can use the estimated value of the flux given by the following equations:

$$\dot{\hat{\Psi}}_\alpha = -R_s i_\alpha + u_\alpha + \nu\eta_\alpha(\psi_{pm}^2 - \eta_\alpha^2 - \eta_\beta^2) \tag{6}$$

$$\dot{\hat{\Psi}}_\beta = -R_s i_\beta + u_\beta + \nu\eta_\beta(\psi_{pm}^2 - \eta_\alpha^2 - \eta_\beta^2) \tag{7}$$

where ν is a positive scalar that establishes the convergence speed of the observer and

$$\eta_\alpha = \hat{\Psi}_\alpha - L i_\alpha \tag{8}$$

$$\eta_\beta = \hat{\Psi}_\beta - L i_\beta \tag{9}$$

The estimated flux $\hat{\Psi}_\alpha$ and $\hat{\Psi}_\beta$ are available for measurement as it only depends on the currents (i_α, i_β) and the voltages (u_α, u_β). Then the estimated rotor position can be given by

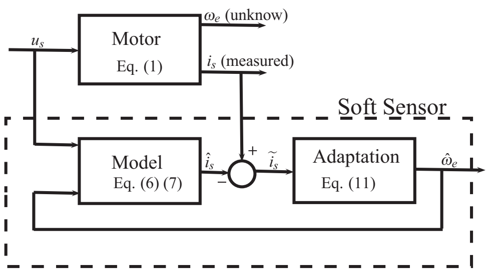

Fig. 2. Block diagram of the soft sensor.

$$\hat{\theta}_e = a\tan 2(\hat{\Psi}_\beta - Li_\beta, \hat{\Psi}_\alpha - Li_\alpha) \tag{10}$$

However, it is not advised to obtain a speed estimate through numerical differentiation of the position estimates. Instead, we use the speed observer given by the following equations [26]:

$$\begin{aligned} \hat{z}_1 &= K_p(\hat{\theta}_e - z_1) + K_i z_2 \\ \hat{z}_2 &= \hat{\theta}_e - z_1 \\ \hat{\omega}_e &= K_p(\hat{\theta}_e - z_1) + K_i z_2 \end{aligned} \tag{11}$$

where K_p and K_i are the proportional and integral gains of the controller, respectively.

The complete soft sensor is shown in Fig. 2 where $i_s = \left[i_\alpha \ i'_\beta\right]$ and $u_s = \left[u_\alpha \ u'_\beta\right]$ represent the stator current vector and the stator voltage vector, respectively.

3. Identification

To ensure that the previously presented sensor works properly the PMSM model and its parameters must be known. For this, a sensorless parameter identification is required. In the automotive application, electrical parameters of PMSM must be identified at standstill before the startup of the motor. The identification process should be fast and requiring a low computing power in order to be incorporated in an electric variator. This paper presents a simple method based on HF signal injection and exploiting the implementation of state variable filters to obtain a linear model with respect to the parameters. Thus, a simplified procedure of identification based on a least squares algorithm can be used to identify the stator resistance and the d- and q-axes inductances of the PMSM.

3.1. Identification method

At standstill, the PMSM can be modeled by the following set of equations:

$$\begin{cases} \hat{u}_d = R_s \hat{i}_d + L_d \dfrac{d\hat{i}_d}{dt} \\ \hat{u}_q = R_s \hat{i}_q + L_q \dfrac{d\hat{i}_q}{dt} \end{cases} \tag{12}$$

By injecting a carrier high-frequency signal, the machine can be considered as a RL load given by the following equations:

$$\hat{u}_{d_H} = R_s \hat{i}_{d_H} + L_d \frac{d\hat{i}_{dH}}{dt} \equiv z_d \hat{i}_{d_H} \tag{13}$$

$$\hat{u}_{q_H} = R_s \hat{i}_{q_H} + L_q \frac{d\hat{i}_{qH}}{dt} \equiv z_q \hat{i}_{q_H} \tag{14}$$

where $\hat{u}_{d_H}$ and $\hat{u}_{q_H}$ are the stator voltages at HF, $\hat{i}_{d_H}$ and $\hat{i}_{q_H}$ are the stator currents at HF, z_d and z_q are the d- and q-axes impedances, respectively, ω_H is the frequency of the injected signal. For a sufficiently high frequency of injection, it can be considered that the stator resistance impedance is negligible compared to the inductances impedances. Then

$$z_d = R_s + j\omega_H L_d \equiv j\omega_H L_d \tag{15}$$

$$z_q = R_s + j\omega_H L_q \equiv j\omega_H L_q \tag{16}$$

In order to estimate the stator resistance R_s and the d-axis inductance L_d, a carrier high-frequency voltage is superimposed to the fundamental frequency voltage along the d-axis:

$$\hat{u}_{d_H} = V_H \cos(\omega_H t) \tag{17}$$

$$\hat{u}_{q_H} = 0 \tag{18}$$

and we obtain

$$\hat{i}_{d_H} = \frac{V_H \cos(\omega_H t)}{z_{d_H} z_{q_H}} \left(z_{moy} - \frac{1}{2} z_{diff} \cos(2\tilde{\theta}_e) \right) \tag{19}$$

$$\hat{i}_{q_H} = -\frac{V_H \cos(\omega_H t)}{z_{d_H} z_{q_H}} \left(\frac{1}{2} z_{diff} \sin(2\tilde{\theta}_e)\right) \tag{20}$$

The stator resistance can be identified at the steady state where the PMSM model is obtained by substituting $d\hat{i}_d/dt = 0$ and $d\hat{i}_q/dt = 0$ into (12). However, the d-axis inductance can be identified at transient state by using the HF model. It should be noted that for a HF voltage injection into the d-axis only L_d can be identified as the used PMSM has a low salience ($z_{diff} = j\omega_H (L_d - L_q) \approx 0$). In this case, the q-axis current $\hat{i}_{q_H}$ is negligible and we cannot estimate L_q. The used model is then

$$\hat{u}_{d_H} = L_d \frac{d\hat{i}_{d_H}}{dt} \tag{21}$$

To estimate the q-axis inductance, a carrier high-frequency voltage is superimposed to the fundamental frequency voltage along the q-axis. So we obtain the following equations:

$$\hat{u}_{d_H} = 0 \tag{22}$$

$$\hat{u}_{q_H} = V_H \cos(\omega_H t) \tag{23}$$

$$\hat{i}_{d_H} = \frac{V_H \cos(\omega_H t)}{z_{d_H} z_{q_H}} \left(-\frac{1}{2} z_{diff} \sin(2\tilde{\theta}_e) \right) \tag{24}$$

$$\hat{i}_{q_H} = \frac{V_H \cos(\omega_H t)}{z_{d_H} z_{q_H}} \left(z_{moy} + \frac{1}{2} z_{diff} \cos(2\tilde{\theta}_e) \right) \tag{25}$$

In this case, the d-axis current $\hat{i}_{d_H}$ is negligible and we cannot estimate L_d. The used model is then

$$\hat{u}_{q_H} = L_q \frac{d\hat{i}_{q_H}}{dt} \tag{26}$$

Therefore, the model can be given by

$$\begin{cases} \hat{u}_d = \hat{R}_s \hat{i}_d \\ \hat{u}_{d_H} = \hat{L}_d \dfrac{d\hat{i}_{d_H}}{dt} \\ \hat{u}_{q_H} = \hat{L}_q \dfrac{d\hat{i}_{q_H}}{dt} \end{cases} \tag{27}$$

At first step, we suppose that we calculate the current derivatives softly. So the general formulation of the recursive least squares (RLS) algorithm used in this paper can be presented as follows:

$$P_k = P_{k-1} - P_{k-1}\underline{\varphi}_k (1 + \underline{\varphi}_k^T P_{k-1} \underline{\varphi}_k)^{-1} \underline{\varphi}_k^T P_{k-1} \tag{28}$$

$$\underline{K}_k = P_{k-1}\underline{\varphi}_k (1 + \underline{\varphi}_k^T P_{k-1} \underline{\varphi}_k)^{-1} \tag{29}$$

$$\hat{\underline{\Theta}}_k = \hat{\underline{\Theta}}_{k-1} + \underline{K}_k [y_k^* - \underline{\varphi}_k^T \hat{\underline{\Theta}}_{k-1}] \tag{30}$$

where $\hat{\underline{\Theta}} = \left[\hat{R}_s \ \hat{L}_d \ \hat{L}_q^T\right]$ is an estimation of $\underline{\Theta} = \left[R_s \ L_d \ L_q\right]^T$ and y_k^* is the measured output ($y_k^* = y_k + b_k$); b_k is the noise for which variance is equal to σ^2. P_0 and $\underline{\Theta}_0$ are the initial values of P_k and

$\underline{\hat{\Theta}}_k$, respectively. If we have no information about the system, we choose $\underline{\Theta}_0 = 0$.

The expression of P_k is provided by the following equation:

$$P_k = \left[\sum_{i=1}^{k} \varphi_i \varphi_i^T \right]^{-1} = (\phi^T \phi)^{-1} \tag{31}$$

with

$$\phi = \begin{bmatrix} \varphi_1^T \\ \varphi_2^T \\ \vdots \\ \varphi_K^T \end{bmatrix} = \begin{bmatrix} \varphi_{11} & \varphi_{12} & \cdots & \varphi_{1N} \\ \varphi_{21} & \varphi_{22} & \cdots & \varphi_{2N} \\ \vdots & \vdots & \ddots & \vdots \\ \varphi_{K1} & \varphi_{K2} & \cdots & \varphi_{KN} \end{bmatrix}$$

The main diagonal of P_k represents the parameters variance given with an accuracy of σ^2. If we have any information about $\underline{\Theta}$, then, its variance is infinite and we choose

$$P_0 = \alpha I = \begin{bmatrix} \alpha & 0 & \dots & 0 \\ 0 & \alpha & \dots & 0 \\ \vdots & \vdots & \ddots & \vdots \\ 0 & 0 & \dots & \alpha \end{bmatrix} \tag{32}$$

with $\alpha \gg 1$. By choosing α small, it means that some degree of confidence is granted to $\underline{\Theta}_0$ and the parameter variation is slow. At the limit, if $\alpha = 0$, then $\underline{\hat{\Theta}}_k$ is constant.

The parameters are estimated one after the other which simplifies the algorithm given by (28)–(30) by avoiding the matrix inversion. The algorithm used for each parameter can be described as follows:

$$\begin{cases} P_{R,k} = P_{R,k-1} - \dfrac{(P_{R,k-1}\hat{i}_d)^2}{1 + P_{R,k-1}\hat{i}_d^2} \\ K_{R,k} = \dfrac{P_{R,k-1}\hat{i}_d}{1 + P_{R,k-1}\hat{i}_d^2} \\ \widehat{R}_{s,k} = \widehat{R}_{s,k-1} + K_{R,k}(\hat{u}_d - \hat{i}_d \widehat{R}_{s,k-1}) \end{cases} \tag{33}$$

$$\begin{cases} P_{1,k} = P_{1,k-1} - \dfrac{\left(P_{1,k-1}\dfrac{d\hat{i}_{d_H}}{dt}\right)^2}{1 + P_{1,k-1}\left(\dfrac{d\hat{i}_{d_H}}{dt}\right)^2} \\ K_{1,k} = \dfrac{P_{1,k-1}\dfrac{d\hat{i}_{d_H}}{dt}}{1 + P_{1,k-1}\left(\dfrac{d\hat{i}_{d_H}}{dt}\right)^2} \\ \hat{L}_{d,k} = \hat{L}_{d,k-1} + K_{1,k}\left(\hat{u}_{d_H} - \dfrac{d\hat{i}_{d_H}}{dt}\hat{L}_{d,k-1}\right) \end{cases} \tag{34}$$

$$\begin{cases} P_{2,k} = P_{2,k-1} - \dfrac{\left(P_{2,k-1}\dfrac{d\hat{i}_{q_H}}{dt}\right)^2}{1 + P_{2,k-1}\left(\dfrac{d\hat{i}_{q_H}}{dt}\right)^2} \\ K_{2,k} = \dfrac{P_{2,k-1}\dfrac{d\hat{i}_{q_H}}{dt}}{1 + P_{2,k-1}\left(\dfrac{d\hat{i}_{q_H}}{dt}\right)^2} \\ \hat{L}_{q,k} = \hat{L}_{q,k-1} + K_{2,k}\left(\hat{u}_{q_H} - \dfrac{d\hat{i}_{q_H}}{dt}\hat{L}_{q,k-1}\right) \end{cases} \tag{35}$$

where

$$P_{R,k-1} = \alpha_R, \quad P_{1,k-1} = \alpha_{L_d}, \quad P_{2,k-1} = \alpha_{L_q}$$

$$\widehat{R}_{s,k-1} = 0, \quad \hat{L}_{d,k-1} = 0, \quad \hat{L}_{q,k-1} = 0$$

To estimate L_d and L_q, we must have the measure of the voltage u_{d_H} and u_{q_H} and calculate the current derivatives $d\hat{i}_{d_H}/dt$ and $d\hat{i}_{q_H}/dt$, respectively. The computing of these derivatives can be a source of problems if the measurement of such currents is noisy. A solution for a safe computation of these derivatives is proposed in Section 4.3.

Fig. 3 shows the progress of parameters identification at standstill, the startup of the motor and the low-speed operation. Initially, we impose a zero velocity to the speed loop and a carrier high-frequency voltage is injected into the d-axis. During the first half second of the injection, the initial rotor position of the motor is estimated. At that moment, we buckle with the estimated speed while keeping the injection of the HF voltage into the d-axis. Between $t = 1$ s and $t = 2.5$ s, we estimate the stator resistance R_s and the d-axis inductance L_d using the recursive least squares method. To identify the stator resistance, we use the steady-state measurements of voltages and currents. However, the HF measurements of voltages and currents are used to estimate L_d. At $t = 3$ s, we stop the injection into the d-axis and we inject the same HF signal into the q-axis. The stator inductance L_q is estimated between $t = 4$ s and $t = 5.5$ s.

3.2. Experimental setup

This section presents the test bench concept that will be used to experimentally validate the performances of the previously designed control scheme. The testbed is composed of two PMSM, connected through a shaft featuring a torque sensor delivering accurate torque measurements. This setup is illustrated in Fig. 4.

These two drives have respective rated power of 1.7 kW and 2.2 kW, and similar rated speed of 6000 rpm. They are intended to deliver a desired torque for the first one, and control the rotary speed of the shaft for the latter. The control strategy previously discussed is implemented in a voltage inverter connected to the first machine. Also note that this machine is equipped with a fine position sensor. This sensor is used to compare the relevancy of the estimated position to the actually measured one, both in operation and at standstill.

3.3. An automotive case study

This test bench allows us to validate the control scheme through *Hardware-in-the-Loop* experiments. Therefore, we consider a vehicular application consisting in a shuttle dedicated to

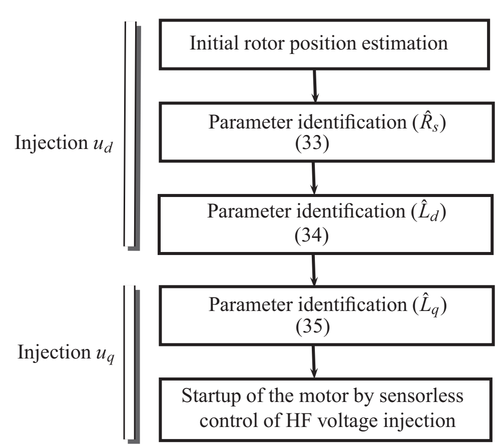

Fig. 3. Flow of parameter identification and low speeds operation.

inner city transportation and featuring a full electric power train including two in-wheel hub motors mounted on the rear axle. These motors are powered by a hybrid energy storage system made up of an arrangement of battery and ultra-capacitor cells, connected in parallel via two boost converters. Further details are given in [29].

3.4. HiL setup

The testbed in Fig. 4 is able to experimentally represent the previous vehicle behavior, by making use of the hardware-in-the-loop (HiL) concept. This bench couples a real motor to mathematical models running in real time to emulate the driveline, the vehicle, as well as the other components such as the battery, the ultracapacitors and the power electronics devices. We use the detailed description provided in [29]. The motor test bench is controlled in such a way that the speed and the torque at the motor output shaft represent the outcome of a driver request (e.g. to follow a prescribed drive cycle). However, since the rated power of the motors are less than the one used in the shuttle, we proceed to use scaling techniques to make the torque and speed trajectories suitable with the PMSM used. This allows us to test the proposed sensorless control scheme in a realistic environment.

Fig. 4. Experimental setup.

3.5. Experimental results

The identification method was tested on the bench presented above. At the beginning, we inject a high frequency voltage $\hat{u}_{d_H}$. At this moment we estimate the resistance (b) and the d-axis inductance (c). Once the identification of R_s and L_d finished, we stop the injection along the d-axis and we inject $\hat{u}_{q_H}$. The identification of the q-axis inductance (d) can be done at that time. Fig. 5 shows the effectiveness of this method where the identified parameters is close to the measured one shown given in Table 1. This method is fast, simple and efficient compared to other methods that involve the use of temperature sensors on the surface of the rotor and in the stator windings, or other techniques requiring a thermal modeling of the machine.

4. Model validation

4.1. Simulation results

In order to be validated, the soft sensor must provide good speed measurements for all the operating points of the motor. Each operating point is defined by the pair $\{\omega_{m0}, T_{L0}\}$ (index 0 indicates steady state operation). The synchronous motor is driven through a Field Oriented Control (FOC) with a model expressed in the rotating frame (d–q). The speed controller imposes the rotor speed ($\omega_m = \omega_m^*$) whatever the load torque (T_L) is provided by the DC motor. PI controllers are used for the control of the currents. The soft sensor provides the speed and

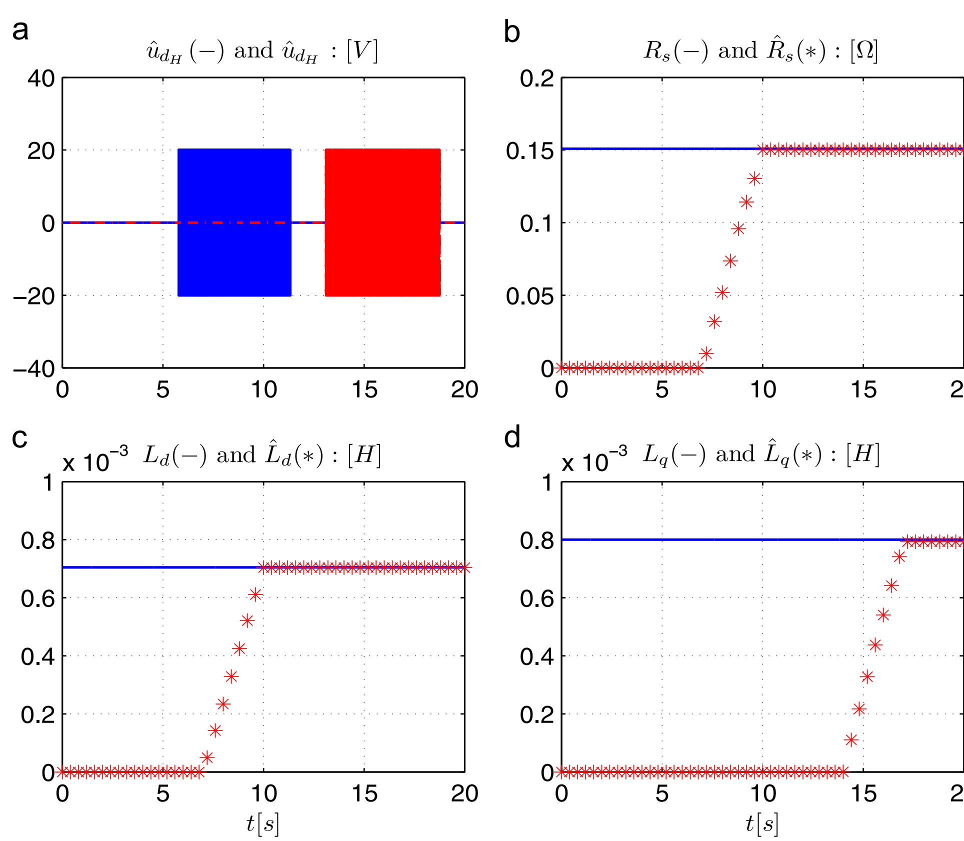

Fig. 5. Identification at standstill. (a) The injected voltages, (b) stator resistance estimation, (c) d-axis inductance estimation L_d, and (d) q-axis inductance estimation L_q.

position estimates $\hat{\omega}_e$ and $\hat{\theta}_e$ which are used in Park's transformation. Fig. 6 presents the block diagram of the sensorless control of a PMSM, whose parameters are shown in Table 1.

The proposed soft sensor is simulated with Matlab/Simulink. Several tests can be performed to investigate the sensor validation, among them, reversal speed at nominal torque and slow load variations at constant speed are particularly used since they correspond to realistic cases. Fig. 7 shows simulation results obtained at the nominal load torque. The speed reference reverses from -120 rpm to 120 rpm. It can be shown that the soft sensor does not provide correct estimation in the whole speed range at nominal torque. In particular, the model diverges from real value at low speed around $\omega_m = 0$. This problem around the zero speed can be explained by the fact that this soft sensor is a model-based sensor. Then, the rotor position estimation depends necessarily on the back-electromotive forces which are proportional to the PMSM speed. So, at low speeds the amplitude of these forces is insignificant which does not allow a perfect estimation of the rotor position. As a solution, HF-based sensors are used at low speed and give a good results as it exploits the saliency of the machine.

4.2. HF-based sensor

The HF-based sensor presented in this section used a carrier high frequency excitation. There are two main forms of carrier high frequency excitation [30]: rotating vector [31–33] and pulsating vector [19,34,35]. The first form injects a balanced three-phase voltage or current carrier signal. If the injected signal is a voltage, then the carrier current response consists of two components: the first one is a positive sequence component which turns in the same direction as the injected voltage vector and the second one is a negative sequence component which turns in the opposite direction. Only the negative component contains the rotor position information. It is necessary to use an appropriate signal processing to extract this component and then estimate the rotor position of the motor. In [33], a simple technique to extract the negative frequency component of the current using only one analog filter is presented. The rotating carrier injection is given by the following equation:

$$\begin{bmatrix} u_{d_H} \\ u_{q_H} \end{bmatrix} = V_H \begin{bmatrix} \cos(\omega_H t) \\ \sin(\omega_H t) \end{bmatrix} \tag{36}$$

The second form injects a voltage or a current carrier signal along the d- or the q-axis. If the injected signal is a voltage, then the carrier current response along the axis orthogonal to the injection axis contains the rotor position information. This method will be detailed later in this section (for more details see [18]). Therefore, a high frequency voltage is added to the d-axis control output as follows:

$$\begin{bmatrix} u_{d_H} \\ u_{q_H} \end{bmatrix} = V_H \begin{bmatrix} \cos(\omega_H t) \\ 0 \end{bmatrix} \tag{37}$$

The carrier current response along the q-axis is then given by:

$$\hat{i}_{q_H} = -\frac{V_H \cos(\omega_H t)}{z_d z_q} \left(\frac{1}{2} z_{diff} \sin(2\tilde{\theta}_e) \right) \tag{38}$$

where

$$\begin{aligned} z_d &= R_s + j\omega_H L_d \\ z_q &= R_s + j\omega_H L_q \\ z_{diff} &= z_d - z_q \end{aligned} \tag{39}$$

For a sufficiently high frequency of injection, it can be considered that the stator resistance impedance is negligible compared to the inductances impedances:

$$\begin{aligned} z_d &= R_s + j\omega_H L_d \equiv j\omega_H L_d \\ z_q &= R_s + j\omega_H L_q \equiv j\omega_H L_q \\ z_{diff} &= j\omega_H L_{diff} = j\omega_H (L_d - L_q) \end{aligned} \tag{40}$$

Then, $\hat{i}_{q_H}$ can be written by

$$\hat{i}_{q_H} = -\frac{V_H \sin(2\tilde{\theta}_e)}{2\omega_H L_{d_H} L_{q_H}} (L_{diff} \sin(\omega_H t)) \tag{41}$$

where $\hat{i}_{q_H}$ depends on the position error $\tilde{\theta}_e$, so a synchronous demodulation is required to calculate the proportional signal to the estimation error of the rotor position. The use of analog filters allows the isolation of the term that contains information about the position and the elimination of undesirable terms. In general, the diagram can be given by Fig. 8. The bandpass filter (BPF) is centered on the carrier frequency f_H. The resulting current is then multiplied by $\sin(\omega_H t)$. At the end, a lowpass filter is used to get

Table 1
Nominal parameters of the synchronous machine.

Features	Values
Pole pair (p)	10
d-axis inductance (L_d)	0.705 mH
q-axis inductance (L_q)	0.8 mH
Stator resistance (R_s)	0.1509 Ω
Permanent magnet flux (ψ_{pm})	8.3 mWb

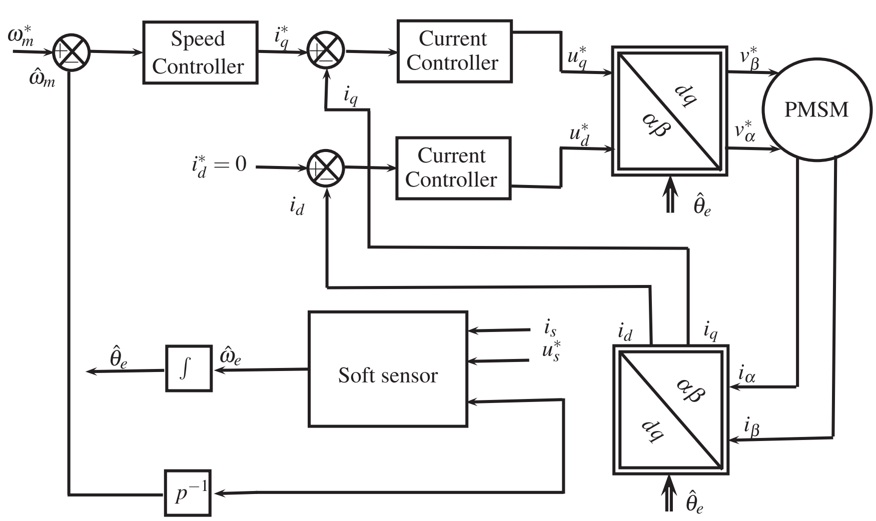

Fig. 6. Block diagram of the soft sensor.

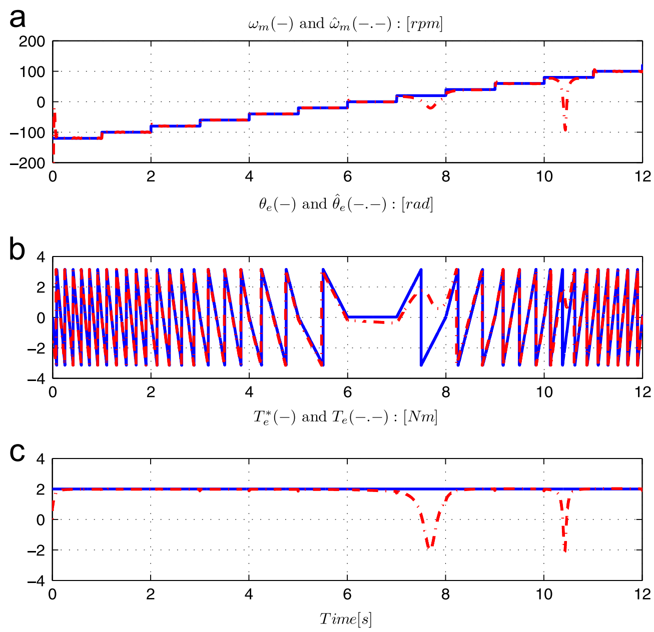

Fig. 7. Simulations: reversal test. Speed varies from -120 rpm to 120 rpm under nominal torque.

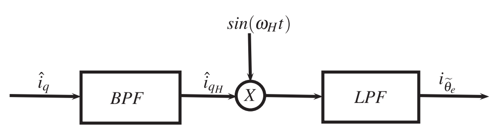

Fig. 8. Demodulation scheme used to obtain the position error signal.

back the signal $i_{\tilde{\theta}_e}$ approached by the following equation:

$$i_{\tilde{\theta}_e} \approx -\frac{V_H L_{diff}}{2\omega_H L_{d_H} L_{q_H}} \tilde{\theta}_e \tag{42}$$

Finally, the rotor speed can be estimated using a PI controller as in [36]

$$\hat{\omega}_e = \chi_p i_{\tilde{\theta}_e} + \chi_i \int i_{\tilde{\theta}_e} \, dt \tag{43}$$

where χ_p and χ_i are the proportional and integral gains of the controller, respectively. The rotor position estimate is given by

$$\hat{\theta}_e = \int \hat{\omega}_e \, dt \tag{44}$$

4.3. Computing time derivatives using state variable filters

As shown in Fig. 8, in the injection techniques, the measurements are filtered by a bandpass filter (BPF) to keep the HF components only. So the idea is to simulate the BPF as a state variable filter (SVF) in order to obtain a safe computation of the current derivatives (Section 3). This filter structure is used for the determination of the current derivatives and therefore the identification of the motor parameters, as well as for the estimation of rotor position and speed in low speed (HF soft sensor). To do this, we consider the BPF given by Eq. (45) which can be written as in (46):

$$H(p) = \frac{b_0 p}{a_0 + a_1 p + a_2 p^2} = \frac{i_f(p)}{i(p)} \tag{45}$$

$$H(p) = \frac{\tau_2 p}{1 + \tau_2 p + \tau_1 \tau_2 p^2} = \frac{i_f(p)}{i(p)} \tag{46}$$

This filter can be simulated as a SVF which can be represented by Fig. 9,

where $I_2 = \frac{1}{\tau_1 p} I_1$ and $I_3 = \frac{1}{\tau_2 p} I_2$.

With this representation, we have $I_2 = i_f$ and $I_1 = \dot{i}_f$. Therefore, the SVF allows us to filter $i(t)$ and to recover directly $i_f(t)$ and $\dot{i}_f(t)$ using only integrators.

By applying the same filter to the voltage $u(t)$, we can identify L ($u_f = L\dot{i}_f$)).

The time constants τ_1 and τ_2 must be calculated according to the characteristics of the BPF (center frequency and bandwidth). The center frequency of this filter corresponds to the frequency of injection.

4.4. Soft sensor design for real-time estimation in a wide speed range including standstill

We have presented above two soft sensors operating in two different ranges of speed. Therefore, it remains to establish a method of transition between both to get a sensorless control in the full-speed range of the permanent magnet synchronous machine.

In this section, we adopt the following notations: $\hat{\omega}_e^{LS}$ and $\hat{\theta}_e^{LS}$ are the estimated speed and position at low speed, respectively, $\hat{\omega}_e^{HS}$ and $\hat{\theta}_e^{HS}$ are the estimated speed and position at high speed, respectively, and $\hat{\omega}_e^{T}$ and $\hat{\theta}_e^{T}$ are the estimated speed and position given by the hybrid observer, respectively. The transition between the two observers, adopted in this paper, has been realized by using weight coefficients W_L and W_H. W_L prevails completely below 80 rpm. However, W_H predominates above 100 rpm.

To determine these coefficients, we tested the performances of the two soft sensors separately. As shown in Fig. 10, the model-based soft sensor does not provide correct estimation at low speed, precisely from -100 rpm to 100 rpm. So we can choose W_H=100. Below 80 rpm, the high frequency soft sensor gives good results so we select W_L=80. The crossing of both algorithms do not affect the estimate of the position, since W_L and W_H are chosen such that $W_L + W_H = 1$, which leads the linear combination to be convex:

$$\hat{\omega}_e^T = W_H \hat{\omega}_e^{HS} + W_L \hat{\omega}_e^{LS} \tag{47}$$

$$\hat{\theta}_e^T = W_H \hat{\theta}_e^{HS} + W_L \hat{\theta}_e^{LS} \tag{48}$$

5. Simulation results

A PMSM with low salience, whose parameters are shown in Table 1, is used for simulation tests. In Fig. 11, we present the block

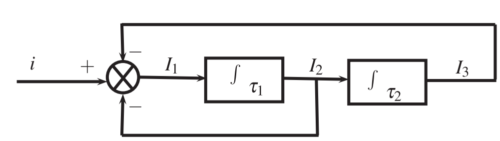

Fig. 9. Block diagram of the state variable filter.

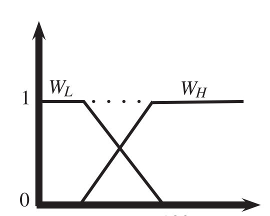

Fig. 10. The transition method.

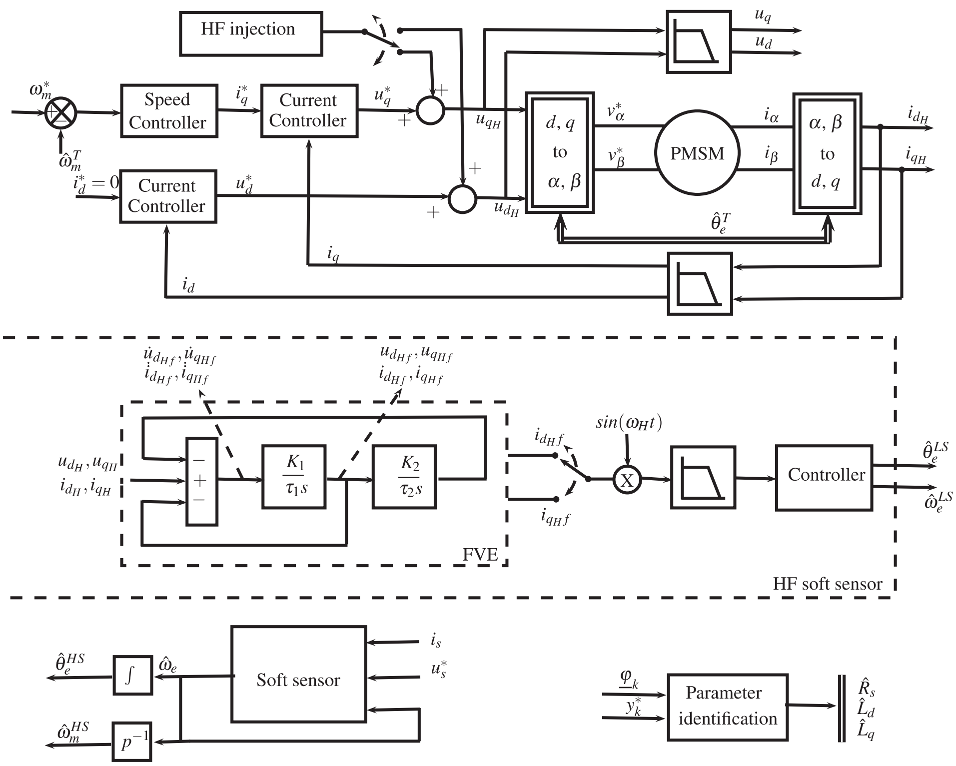

Fig. 11. Block diagram of the soft sensor: identification at standstill, operation at low and high speed and transition between the two speed ranges.

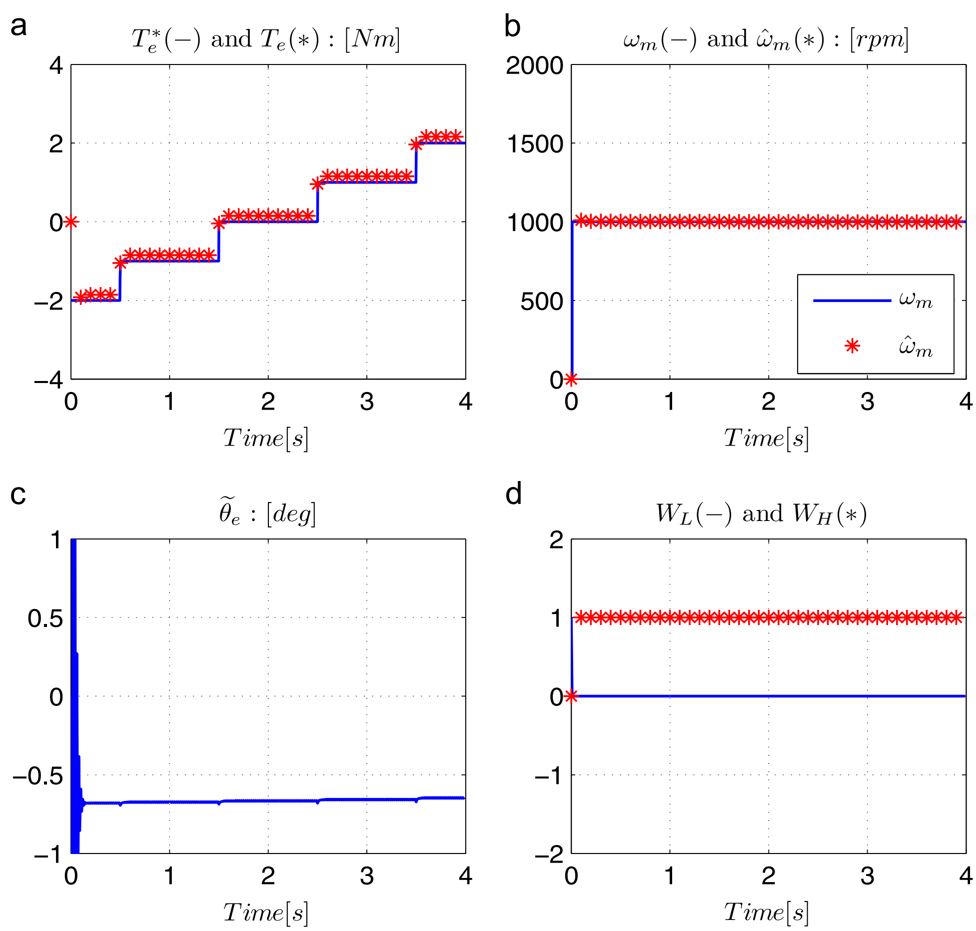

Fig. 12. Simulation results with torque variations and constant speed $\omega_m = 1000$ rpm.

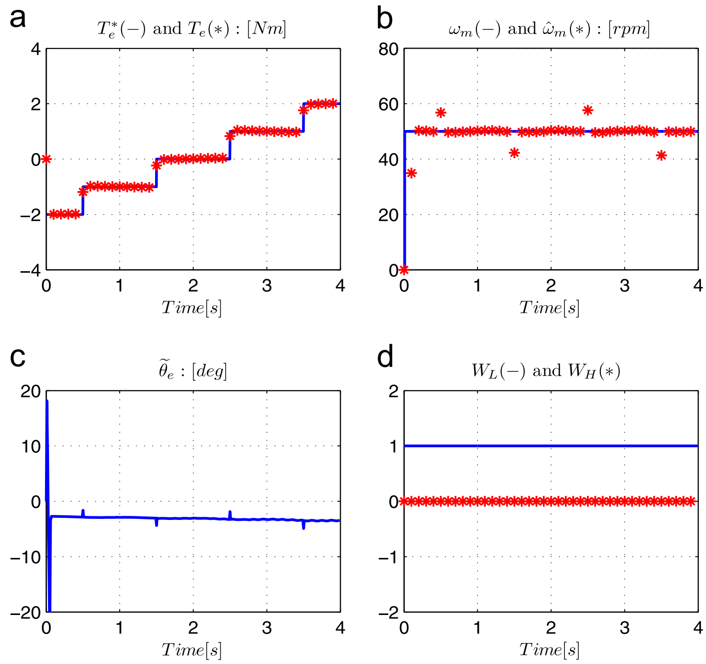

Fig. 13. Simulation results with torque variations and constant speed $\omega_m = 50$ rpm.

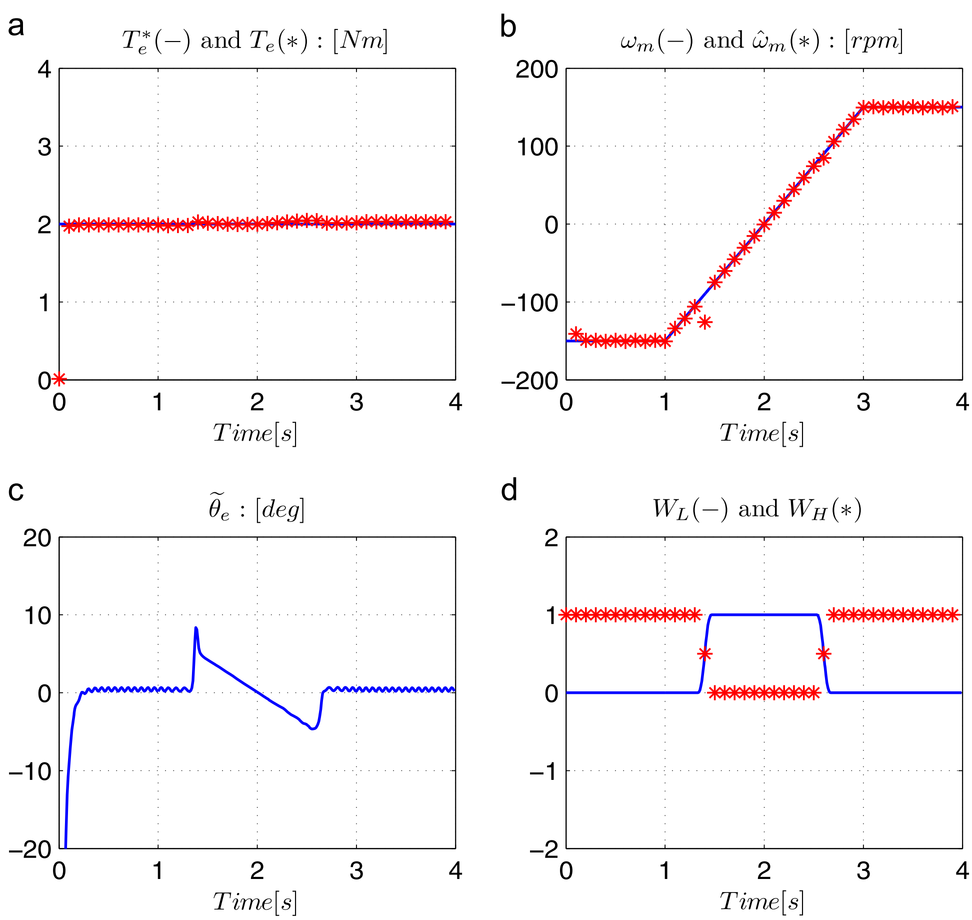

Fig. 14. Simulation results during a speed reversal test under constant load $T_e = 2$ N m.

diagram of the sensorless control system of PMSM with online parameter identification at standstill and operation at low speeds and high speeds where a cascaded speed and current control loops are shown. PI controllers are used for the regulation of the currents. In this scheme, state variable filters are used as bandpass filters in the signal injection method and enables us to calculate the currents derivatives used in the parameters identification. The proposed hybrid sensor was investigated in simulation for different cases. Figs. 12 and 13 show the PMSM torque, the PMSM speed, the position estimation error and the two weight coefficients

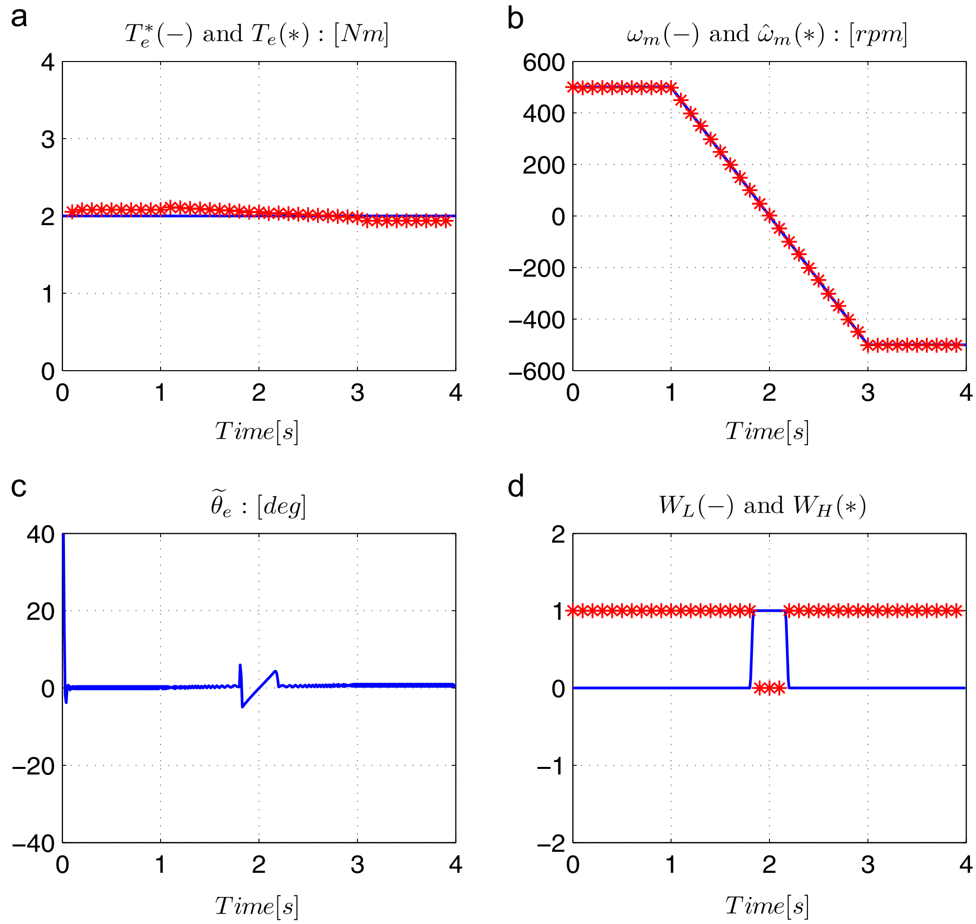

Fig. 15. Simulation results during a speed reversal test under constant load $T_e = 2$ N m.

W_L and W_H at high and low speed while the torque request is varied from -2 N m to 2 N m. Fig. 12 shows the performance of the model-based soft sensor at 1000 rpm. In this case the HF-based sensor is not involved in the speed and the position estimation of the machine. For this, we have $W_L=0$ and $W_H=1$. It can be seen that the estimated speed tracks the actual speed very well and the position estimation error does not exceed 0.7°. In Fig. 13, only the HF-based sensor is involved in the estimation where $W_L=1$ and $W_H=0$. The presented results prove the efficiency of the proposed soft sensor at low speed. The performance of the hybrid soft sensor in a wide speed range including the standstill has been investigated. The results are shown in Figs. 14 and 15 where the machine was reversed from -150 to 150 rpm and from 500 to -500 rpm, respectively. It can be seen that the switching between the model-based soft sensor and the HF-based sensor was performed smoothly without any problem. High frequency signal injection was activated from the standstill until 80 rpm to estimate the position and the speed at low speed, between 80 and 100 rpm a smooth transition was imposed. Beyond 100 rpm the injected signal was removed and only the model-based sensor is used. Simulation results show the relevancy of the proposed hybrid soft sensor. It can be concluded that this soft sensor is simple, efficient and a suitable candidate for practical implementation.

6. Conclusion

In this paper, we have presented the complete design of a soft sensor for speed measurement of permanent magnet synchronous motor. The rotor speed and position can be estimated in a wide speed range even at low speed and standstill. We have introduced two soft sensors operating in two different ranges of speed. Also, a method of transition between both has been presented. Simulation results showed the robustness of the proposed sensor.

Acknowledgments

This work has been supported by IFP Energies Nouvelles, Paris, France.

References

[1] Abdelli R, Rekioua D, Rekioua T. Performances improvements and torque ripple minimization for VSI fed induction machine with direct control torque. ISA Trans 2011;50:213–9.
[2] Achour AY, Mendil B, Bacha S, Munteanu I. Passivity-based current controller design for a permanent-magnet synchronous motor. ISA Trans 2009;48:336–46.
[3] Zhang B, Pi Y, Luo Y. Fractional order sliding-mode control based on parameters auto-tuning for velocity control of permanent magnet synchronous motor. ISA Trans 2012;51:649–56.
[4] Bogaerts Ph, VandeWouwer A. Software sensors for bioprocesses. ISA Trans 2003;42:547–58.
[5] Escobar RF, Astorga-Zaragoza CM, Tellez-Anguiano AC, Juarez-Romero D, Hernandez JA, Guerrero-Ramirez GV. Sensor fault detection and isolation via high-gain observers: application to a double-pipe heat exchanger. ISA Trans 2011;50:480–6.
[6] Vijaya Raghavana SR, Radha krishnan TK, Srinivasan K. Soft sensor based composition estimation and controller design for an ideal reactive distillation column. ISA Trans 2011;50:61–70.
[7] Kubota H, Matsuse K. DSP-based speed adaptive flux observer of induction motor. IEEE Trans Ind Appl 1993;29:344–8.

[8] Karimia HR, Babazadehb A. Modeling and output tracking of transverse flux permanent magnet machines using high gain observer and RBF neural network. ISA Trans 2005;44:445–56.
[9] Hinkkanen M, Harnefors M, Luomi J. Reduced-order flux observers with stator-resistance adaptation for speed-sensorless induction motor drives. IEEE Trans Power Electron 2010;25:1173–83.
[10] Zheng S, Tang X, Song B, Lu S, Ye B. Stable adaptive PI control for permanent magnet synchronous motor drive based on improved JITL technique. ISA Trans 2013;52:539–49.
[11] Yang G, Chin T. Adaptive-Speed identification scheme for a vector-controlled speed sensorless inverter-induction motor drive. IEEE Trans Ind Appl 1993;29:820–5.
[12] Madadi-Kojabadi G. Simulation and experimental studies of model reference adaptive system for sensorless induction motor drive. Simul Model Pract Theory 2005;13:451–64.
[13] Orlowska-Kowalska T, Dybkowski M. Stator-current-based MRAS estimator for a wide range speed-sensorless induction-motor drive. IEEE Trans Ind Electron 2010;57:1296–308.
[14] Xu D, Zhang S, Liu J. Very-low speed control of PMSM based on EKF estimation with closed loop optimized parameters. ISA Trans 2013;52:835–43.
[15] Etien E. Modeling and simulation of soft sensor design for real-time speed estimation, measurement and control of induction motor. ISA Trans 2013;52:358–64.
[16] DeBelie FM, Sergeant P, Melkebeek JA. A sensorless PMSM drive using modified high-frequency test pulsesequences for the purpose of a discrete-time current controller with fixedsampling frequency. J Math Comput Simul 2010;81:367–81.
[17] Leidhold R. Position sensorless control of PM synchronous motors based on zero-sequence carrier injection. IEEE Trans Ind Electron 2011;58:5371–9.
[18] Jang J, Sul S, Ha J, Ide K, Sawamura M. Sensorless drive of surface-mounted permanent-magnet motor by high-frequency signal injection based on magnetic saliency. IEEE Trans Ind Appl 2003;39:1031–9.
[19] Choi CH, Seok JK. Pulsating signal injection-based axis switching sensorless control of surface-mounted permanent-magnet motors for minimal zero-current clamping effects. IEEE Trans Ind Appl 2008;344:1741–8.
[20] Piippo A, Hinkkanen M, Luomi J. Adaptation of motor parameters in sensorless PMSM drives. IEEE Trans Ind Appl 2009;45:203–12.
[21] Sayeef S, Foo G, Rahman MF. Rotor position and speed estimation of a variable structure direct-torque-controlled IPM synchronous motor drive at very low speeds including standstill. IEEE Trans Ind Electron 2010;57:3715–23.
[22] Omrane I, Dib W, Etien E, Bachelier O. Sensorless control of PMSM based on a nonlinear observer and a high-frequency signal injection for automotive applications. In: The 39th annual conference of the IEEE industrial electronics society IECON, Vienna, Austria; 2013.
[23] J-I Ha, Kang S-J, Sul S-K. Position-controlled synchronous reluctance motor without rotational transducer. IEEE Trans Ind Appl 2006;35:1393–8.
[24] Bolognani S, Faggion A, Fornasiero E, Sgarbossa L. Full speed range sensorless IPM motors drives. In: International conference on electrical machines ICEM, Marseille, France; 2012.
[25] Silva C, Asher GM, Sumner M. Hybrid rotor position observer for wide speed-range sensorless PM motor drives including zero speed. IEEE Trans Ind Electron 2006;53:373–8.
[26] Lee J, Hong J, Nam K, Ortega R, Praly L, Astolfi A. Sensorless control of surface-mount permanent-magnet synchronous motors based on a nonlinear observer. IEEE Trans Power Electron 2010;25:290–7.
[27] Ortega R, Praly L, Astolfi A, Lee J, Nam K. Estimation of rotor position and speed of permanent magnet synchronous motors with guaranteed stability. IEEE Trans Control Syst Technol 2010;19:601–14.
[29] Malaizé J, Dib W. A sensorless-based control scheme to enhance the accuracy of position encoders used in permanent magnet synchronous motors for automotive applications. Society of Automotive Engineers (SAE); 2012.
[30] Garcia P, Guerrero JM, El-Sayed I, Briz F, Reigosa D. Carrier signal injection alternatives for sensorless control of active magnetic bearings. In: Symposium on sensorless control for electrical drives SLED, Padova, Italy; 2010.
[31] Linke M, Kennel R, Holtz J. Sensorless position control of permanent magnet synchronous machines without limitation at zero speed. In: The 28th annual conference of the IEEE industrial electronics society IECON, Sevilla, Spain; 2002.
[32] Saltiveri D, Arias A, Asher G, Sumner M, Wheeler P, Empringham L, et al. Sensorless control of surface-mounted permanent magnet synchronous motors using matrix converters. J Electr Power Qual Util 2006;12:59–67.
[33] Mansouri-Toudert O, Zeroug H, Auger F, Chibah A. Improved rotor position estimation of salient-pole PMSM using high frequency carrier signal injection. In: International conference on electrical machines ICEM, Marseille, France; 2012.
[34] Ha J, Ide K, Sawa T, Sul S. Sensorless rotor position estimation of an interior permanent-magnet motor from initial states. IEEE Trans Ind Appl 2003;39:761–7.
[35] Hammel W, Kennel RM. Position sensorless control of PMSM by synchronous injection and demodulation of alternating carrier voltage. In: Symposium on sensorless control for electrical drives SLED, Padova, Italy; 2010.
[36] Piippo A, Hinkkanen M, Luomi J. Adaptation of motor parameters in sensorless PMSM drives. IEEE Trans Ind Appl 2009;45:203–12.